CrossMark

ORIGINAL PAPER

Stress Wave Propagation Across a Rock Mass with Two Non-parallel Joints

S. B. Chai[1] · J. C. Li[2] · Q. B. Zhang[3] · H. B. Li[1] · N. N. Li[1]

Abstract A rock mass includes a number of joints, which govern the mechanical behavior of the rock mass and greatly affect stress wave propagation. Generally, joints do not parallel with each other, resulting in multiple wave reflections between joints and complex wave propagation process in rock masses. The present study presents an approach to analyze stress wave propagation through a rock mass with two non-parallel joints when the angle between the two joints is <10°. For incident P-wave impinging on this kind of rock mass, multiple reflections take place between the two joints. Meanwhile, transmitted waves are generated and propagate successively away from the joints. The mathematical expressions for P-wave propagation across the two joints are established in time domain by analyzing the wave field in the rock mass. By comparing with the result from numerical simulation, the new approach is proved to be effective to analyze wave propagation across two non-parallel joints, where the influence of joint tips on wave propagation is neglected. Parametric studies show that the joint stiffness, joint angle and frequency of incident wave have different effects on transmission and reflection coefficients.

List of Symbols

k_{n1} and k_{s1}	Normal and tangential stiffness of joint J1, respectively
k_{n2} and k_{s2}	Normal and tangential stiffness of joint J2, respectively
c_p and c_s	P- and S-wave propagation velocities, respectively
I_p and I_s	Incident P- and S-waves, respectively
T_p and T_s	Transmitted P- and S-waves, respectively
R_p and R_s	Reflected P- and S-waves, respectively
v_i	Particle velocity, where the subscript i represents the wave type
t	Time
z_p and z_s	Wave impedances of P- and S-waves, respectively
ρ	Rock density
T_x and T_y	Horizontal and vertical components of transmission coefficient, respectively
R_x and R_y	Horizontal and vertical components of reflection coefficient
A_I	Amplitude of incident wave
f	Frequency of incident wave
ω	Angular frequency
K_n and K_s	Normalized normal and tangential stiffness, respectively
α_1 and α_2	Angles between the two joints and x-axis, respectively
α and β	Emergence angles of P- and S-waves, respectively
θ_{pcr} and θ_{scr}	Critical angles of P- and S-waves, respectively

✉ J. C. Li
  jcli@seu.edu.cn

[1] State Key Laboratory of Geomechanics and Geotechnical Engineering, Institute of Rock and Soil Mechanics, Chinese Academy of Sciences, Wuhan 430071, China

[2] School of Civil Engineering, Southeast University, Nanjing, China

[3] Department of Civil Engineering, Monash University, Building 60, Clayton, VIC 3800, Australia

θ_i^j (j = J1 and J2)	Emergence angle of waves from the joint, where the subscript i denotes the wave type and superscript j denotes the joint
$\theta_i^{x_i}$	Angles between the waves and vertical direction, where subscript i denotes the wave type
L_i	Traveling distance of stress wave, where the subscript i denotes the wave type
X	Abscissa
x_i	Horizontal coordinate of a point in the numerical model
Δx	Horizontal distance between two adjacent points
q	Point number

1 Introduction

Joints widely exist in rock masses and greatly affect stress wave propagation. The interaction between stress waves and rock joints is an important issue in rock engineering. Theoretical and numerical methods have widely been adopted to study wave propagation in a jointed rock mass.

The equivalent medium method (EMM) and the displacement discontinuity method (DDM) are two typical theoretical methods. Generally, the EMM treats the joints as a part of rock medium with effective moduli so that the rock mass can be regarded as a continuous medium (Schoenberg and Muir 1989; Cook 1992). A viscoelastic equivalent medium method coupled with the virtual wave source method was proposed to effectively analyze the process of multiple wave reflections between parallel joints for one-dimensional problem (Li et al. 2010). The virtual wave source method was then modified to show the multiple wave reflections for wave propagation across parallel joints with arbitrary incident angle (Zhu et al. 2011). Later, Ma et al. (2012) improved the viscoelastic equivalent medium method for investigating wave propagation across nonlinear joints. In the DDM, each joint is taken as a non-welded interface on which the stress is continuous, while the displacement is discontinuous (Schoenberg 1980). Based on the DDM, Pyrak-Nolte et al. (1990a) analyzed wave transmission characters across a single dry or fully liquid-filled joint. Pyrak-Nolte et al. (1990b) derived the closed-form solutions in a matrix form for a harmonic incident wave across a linear fracture. When the method of characteristic (MC) (Achenbach 1973; Cai and Zhao 2000) was combined, the DDM became an effective analytical method to study P- and S-wave propagation normally across a single or a set of parallel nonlinear joints (Zhao and Cai 2001; Zhao et al. 2006). The DDM combined with MC was then applied to separately analyze the effects of in situ stress (Fan and Sun 2015) and unequal close–open behavior of joints (Li et al.

2016) on wave propagation. Zhu et al. (2012) adopted a modified recursive method to analyze multiple wave reflections among parallel joints filled with viscoelastic medium. Perino et al. (2012) adopted the scattering matrix method (SMM) to analyze wave propagation across elastic and/or viscoelastic joints. Li et al. (2012) proposed a time-domain recursive method (TDRM), which considers the compatibility condition at joint interfaces to establish a wave propagation equation in time differential form for stress wave propagating across a linear joint set with arbitrary emergence angle. The TDRM was later extended to analyze wave propagation across nonlinear joints (Li 2013).

Numerical modeling is an alternative way to study wave propagation besides theoretical and experimental methods, especially when the theoretical solutions are impossible to be obtained and experiments are difficult to be conducted. For example, Chen and Zhao (1998) simulated the wave propagation and dynamic responses of a rock mass with joints under explosive loading. Zhao et al. (2008) modeled the stress wave vertically propagating along linear and nonlinear joints and obtained the relationship of interaction between stress waves and joints. The numerical ones were then compared with their experimental results. The commonly used numerical modeling methods include the finite element method (FEM) (e.g., Goodman et al. 1968), the boundary element method (BEM) (Crotty and Wardle 1985) and the discrete element method (DEM) (Cundall 1971). The FEM, i.e., a continuum-based method, takes the joint as a special unit, while a joint is regarded as a boundary surface in the BEM analysis. The first two methods are incapable of dealing with many intersecting interfaces and have limitations including small displacements of joints and small rotations of discrete rock blocks which restrict their applications in discontinuous problems. Compared with the other two numerical methods, DEM has some advantages such as well-developed theories and more easily handleable softwares. The universal discrete element code (UDEC), i.e., a sort of software based on DEM, has been proved to be accurate and efficient to simulate wave propagation across in jointed rock masses (e.g., Chen and Zhao 1998; Zhao et al. 2008; Zhu et al. 2013).

In nature, joints commonly exist in a rock mass with arbitrary distribution pattern. When a stress wave impinges on joints, the transmission and reflection from joints as well as multiple reflections between joints take place. The split Hopkinson pressure bar (SHPB) tests carried out by Wu et al. (2013, 2014) showed that the process of multiple reflections between two discontinuous boundaries is complicated. Wave propagation across non-parallel joints is more complex. Theoretical analyses for stress wave interaction with non-parallel rock joints have less been reported. The intention of the study is to analyze wave propagation across two non-parallel rock joints and to better understand the effects

of influence factors on wave propagation. The incident wave is assumed to be a longitudinal (P-) wave. In the study, the stress wave transmitting and reflecting processes between the two non-parallel joints are first investigated. The wave propagation equations are then established from the wave field between and outside the two joints. After that, verification is conducted by comparing two kinds of results from the analytical method and numerical simulation method. Finally, the effects of some parameters, such as the joint stiffness, joint angle and the frequency of incident wave, on wave propagation are analyzed, respectively.

2 Methodology

2.1 Problem Description

Assume that there are two non-parallel joints (denoted as J1 and J2) in a rock mass, as shown in Fig. 1. The joints are in the x–z plane and extend largely in the x–y plane. The angles between the two joints and the x-axis (e.g., the horizontal direction) are α_1 and α_2, respectively. When an incident plane P-wave impinges on the joints, wave transmission and reflection take place at the joints.

The rocks on both sides of the joints are assumed to be elastic, homogeneous and isotropic. The joints are linearly elastic, and the normal and tangential stiffness are k_{n1} and k_{s1}, respectively, for J1, and k_{n2} and k_{s2}, respectively, for J2. The incident P-wave propagates upward and along the axis y, as shown in Fig. 1.

The process of wave propagation across the two joints includes three portions: incident wave impinging on and reflected from J1, multiple reflections between two joints, and transmitted waves from J2. The rock mass with two non-parallel joints can be divided into three zones, i.e., Zone I, II and III in Fig. 1, according to the wave propagation process. The waves in Zone I include three groups, i.e., (1) the incident P-waves; (2) the waves reflected from J1; (3) the transmitted waves when multiple waves in Zone

II impinge on J1. In Zone II, there exist multiple waves transmitted from J1 and reflected between J1 and J2. The waves in Zone III are only the transmitted waves from J2. Accordingly, for the rock mass containing two non-parallel joints, the waves in Zone III can be supposed to be the transmitted waves, and the waves in Zone I except the incident P-waves can represent the reflected waves.

Besides the three zones of wave field, the tip of each joint causes stress concentration during wave propagation around the tip. In this study, we focus on studying wave propagation before and after the joints, so that the effect of joint tip is neglected.

2.2 Wave Propagation Across a Single Joint

When a P- or S-wave impinges on a rock joint, both reflection and transmission take place, as shown in Fig. 2, where I_p or I_s denotes the incident wave, R_p and R_s denote the reflected P- and S-waves, respectively, and T_p and T_s denote the transmitted P- and S-waves, respectively. The symbols α and β represent the emergence angles of P- and S-waves, respectively. The waves satisfy the Snell's law; therefore, there is $\sin \beta / \sin \alpha = c_s / c_p$, where c_p and c_s are the propagation speeds of P- and S-waves, respectively, and α and β are the emergence angles of P- and S-waves, respectively. Based on the DDM and the compatibility condition at joint interfaces, Li et al. (2012) derived the wave propagation equations in the time domain for two-dimensional problems by analyzing the relation between stress wave and a single rock joint. The equations can be expressed as:

$$\begin{bmatrix} v_{Rp} \\ v_{Rs} \end{bmatrix}_{(i)} = -B^{-1}A_m v_{Im(i)} + B^{-1}C \begin{bmatrix} v_{Tp} \\ v_{Ts} \end{bmatrix}_{(i)} \quad (1)$$

$$\begin{bmatrix} v_{Tp} \\ v_{Ts} \end{bmatrix}_{(i+1)} = G^{-1}D v_{Im(i)} + G^{-1}E \begin{bmatrix} v_{Rp} \\ v_{Rs} \end{bmatrix}_{(i)} + G^{-1}F \begin{bmatrix} v_{Tp} \\ v_{Ts} \end{bmatrix}_{(i)} \quad (2)$$

where v_{Rp} and v_{Tp} denote the particle velocities of the reflected and transmitted P-waves, respectively; v_{Rs} and v_{Ts} denote the particle velocities of the reflected and
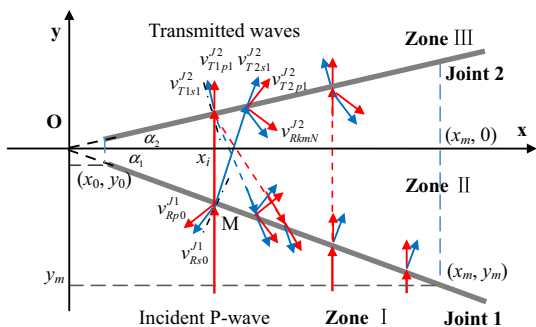

Fig. 1 Schematic view of wave propagation between two non-parallel joints
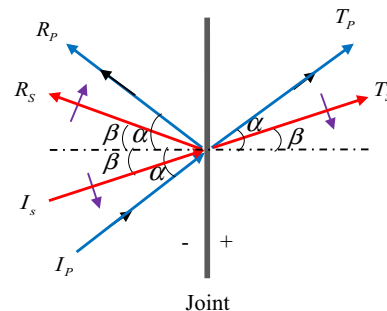

Fig. 2 Schematic view of incident, reflected and transmitted waves on a single rock joint

transmitted S-waves, respectively. v_{Im} is the particle velocity of the incident wave, and m is p or s, representing the wave type. The matrix parameters A to G are written as

$$A_p = \begin{bmatrix} z_p \cos(2\beta) \\ z_p \sin(2\beta) \tan\beta / \tan\alpha \end{bmatrix}, \tag{3}$$

$$A_s = \begin{bmatrix} z_s \sin(2\beta) \\ -z_s \cos(2\beta) \end{bmatrix}, \tag{4}$$

$$B = \begin{bmatrix} z_p \cos(2\beta) & -z_s \sin(2\beta) \\ -z_p \sin(2\beta) \tan\beta / \tan\alpha & -z_s \cos(2\beta) \end{bmatrix}, \tag{5}$$

$$C = \begin{bmatrix} z_p \cos(2\beta) & z_s \sin(2\beta) \\ z_p \sin(2\beta) \tan\beta / \tan\alpha & -z_s \cos(2\beta) \end{bmatrix}, \tag{6}$$

$$D = \begin{bmatrix} k_n \Delta t \cos\alpha \\ k_s \Delta t \sin\alpha \end{bmatrix}, \tag{7}$$

$$E = \begin{bmatrix} -k_n \Delta t \cos\alpha & k_n \Delta t \sin\beta \\ k_s \Delta t \sin\alpha & k_s \Delta t \cos\beta \end{bmatrix}, \tag{8}$$

$$F = \begin{bmatrix} -k_n \Delta t \cos\alpha + z_p \cos(2\beta) & -k_n \Delta t \sin\beta + z_s \sin(2\beta) \\ -k_s \Delta t \sin\alpha + z_p \sin(2\beta) \tan\beta / \tan\alpha & k_s \Delta t \cos\beta - z_s \cos(2\beta) \end{bmatrix}, \tag{9}$$

$$G = \begin{bmatrix} z_p \cos(2\beta) & z_s \sin(2\beta) \\ z_p \sin(2\beta) \tan\beta / \tan\alpha & -z_s \cos(2\beta) \end{bmatrix} \tag{10}$$

In the matrix parameters, z_m (m is p or s) denotes the seismic wave impedance of P- or S-wave in the intact rock and equals to ρc_m. Equations (1) and (2) will be used for wave propagation across one joint with arbitrary emergence angle.

2.3 Wave Propagation Between Two Non-parallel Joints

As shown in Fig. 1, the intersection of the extensions of the two joints is at the coordinate origin O. The scope of the monitoring abscissa is $x_i \in (x_0, x_m)$. Assume there is an incident P-wave with wave front at $y = y_m$. When the incident wave arrives at one point M with coordinate (x_i, y_i) on the joint J1, the traveling distance is

$$L_I = (x_m - x_i)\tan\alpha_1 \tag{11}$$

If the incident P-wave at $y = y_m$ is denoted as $v_0(t)$, the incident wave arriving at M can be written as

$$v_{I0}(t) = v_0(t - L_I/c_p) \tag{12}$$

When the incident wave propagates one distance and impinges on J1, the incident angle is α_1, the emergence angles of both transmitted and reflected P-waves from J1 are α_1, and the emergence angles of both transmitted and reflected S-waves produced from J1 are β_1. Since the plane P- and S-waves across J1 satisfy the Snell's law, i.e., $\beta_1 = \sin^{-1}[\sin(\alpha_1)c_s/c_p]$, the reflected P- and S-waves from J1

and the transmitted waves from J1 can be obtained from the wave propagation equation across a single joint introduced in Sect. 2.2. The P- and S-waves reflected from J1 will then propagate downward away from J1. The reflected waves from J1 are denoted as $v_{Rm0}^{J1}(t)$, where the subscript m is p or s denoting for the reflected P- and S-waves, respectively.

The angle between the reflected P-wave and the axis y (e.g., the vertical direction) is $2\alpha_1$, and the angle between the reflected S-wave and the y-axis is $\alpha_1 + \beta_1$. Therefore, the vertical and horizontal components of the particle velocity caused by the two reflected waves can be derived as

$$\begin{cases} v_{Rpy}^{x_i}(x, t) = -\cos 2\alpha_1 \cdot v_{Rp0}^{J1}(t) \\ v_{Rpx}^{x_i}(x, t) = -\sin 2\alpha_1 \cdot v_{Rp0}^{J1}(t) \\ v_{Rsy}^{x_i}(x, t) = \sin(\alpha_1 + \beta_1) \cdot v_{Rs0}^{J1}(t) \\ v_{Rsx}^{x_i}(x, t) = -\cos(\alpha_1 + \beta_1) \cdot v_{Rs0}^{J1}(t) \end{cases} \tag{13}$$

where the superscript x_i denotes the abscissa of one point on J1 and the variable parameter x in parentheses presents the abscissa of the emergence points of each reflected waves. The transmitted P- and S-waves generated from J1, $v_{Tp0}^{J1}(t)$ and $v_{Ts0}^{J1}(t)$, then become new incident waves and propagate toward the joint J2. The newly generated incident waves impinging on J2 are written as

$$v_{ImN}^{J2}(t) = v_{Tm0}^{J1}(t - L_{m0}^{J1}/c_m) \tag{14}$$

where the subscript N denotes the times of interaction between the wave and joint. The traveling distance of the new incident wave between the two joints is denoted as $L_{m0}^{J1}(t)$. If the waves are only caused by the incident wave, N is equal to one. The emergence angles of the newly generated incident P- and S-waves arriving at J2 are α_2 and $\alpha_1 + \alpha_2 - \beta_1$, respectively. When the normal and shear stiffness of J2 are known, the transmitted and reflected waves generated from J2 can be calculated from Eqs. (1) and (2). The induced four types of transmitted waves are denoted as v_{TkmN}^{J2} ($m = p, s; k = 1, 2$), which is shown in Fig. 1. In Zone III, the transmitted P- and S-waves generated from J2 are expressed as

$$v_{Tm}^{x_i}(x, t) = v_{TkmN}^{J2}(t) \tag{15}$$

where x denotes the abscissa of a point on J2. When k are 1 and 2, x are x_i and $x_i[1 + \tan\alpha_1\tan(\alpha_1 - \beta_1)]$, respectively. Since the waves impinging on and generated from J2 also satisfy the Snell's law, the emergence angles of the four transmitted P- and S-waves, θ_{TkmN}^{J2}, can be obtained and written as $\sin^{-1}(\sin\alpha_2 \cdot c_s/c_p)$, α_2, $\alpha_1 + \alpha_2 - \beta_1$ and $\sin^{-1}(\sin(\alpha_1 + \alpha_2 - \beta_1) \cdot c_p/c_s)$, respectively. The angles between the transmitted P- and S-waves and the axis y are

$$\theta_{Tm}^{x_i}(x) = \theta_{TkmN}^{J2} - \alpha_2 \tag{16}$$

From Eqs. (15) and (16), the vertical and horizontal components of each transmitted wave from J2 can be expressed as

$$\begin{bmatrix} v_{\mathrm{Tp}y}^{x_i}(x,t) \\ v_{\mathrm{Tp}x}^{x_i}(x,t) \end{bmatrix} = v_{\mathrm{Tp}}^{x_i}(x,t) \cdot \begin{bmatrix} \cos\theta_{\mathrm{Tp}}^{x_i}(x) \\ \sin\theta_{\mathrm{Tp}}^{x_i}(x) \end{bmatrix} \quad (17)$$

$$\begin{bmatrix} v_{\mathrm{Ts}y}^{x_i}(x,t) \\ v_{\mathrm{Ts}x}^{x_i}(x,t) \end{bmatrix} = v_{\mathrm{Ts}}^{x_i}(x,t) \cdot \begin{bmatrix} -\sin\theta_{\mathrm{Ts}}^{x_i}(x) \\ \cos\theta_{\mathrm{Ts}}^{x_i}(x) \end{bmatrix} \quad (18)$$

The four reflected waves from J2, denoted as $v_{\mathrm{R}kmN}^{\mathrm{J2}}$, become newly generated incident waves and repeatedly propagate between the two joints. After traveling a certain distance, L_{kmN}^{J2}, the newly generated four incident waves arrive at J1. At this moment, the four waves are written as

$$v_{\mathrm{I}kmN}^{\mathrm{J1}}(t) = v_{\mathrm{R}kmN}^{\mathrm{J1}}\big(t - L_{kmN}^{\mathrm{J2}}/c_m\big), \quad (m = p, s; \; k = 1, 2) \quad (19)$$

and the incident angle of each wave impinging on J1 is

$$\theta_{\mathrm{I}kmN}^{\mathrm{J1}} = \alpha_1 + \alpha_2 + \theta_{\mathrm{R}kmN}^{\mathrm{J2}} \quad (20)$$

where $\theta_{\mathrm{R}kmN}^{\mathrm{J2}}$ denotes the emergence angle of the reflected waves from J2, which is equal to the emergence angles, $\theta_{\mathrm{T}kmN}^{\mathrm{J2}}$, of the four transmitted P- and S-waves from J2. The critical angles of P- and S-waves are denoted by $\theta_{m\mathrm{cr}}$. Since the media beside each joint are identical, there are $\theta_{\mathrm{pcr}} = 90°$ and $\theta_{\mathrm{scr}} = \sin^{-1}(c_s/c_p)$. Supposing $\theta_{\mathrm{I}kmN}^{\mathrm{J1}} < \theta_{m\mathrm{cr}}$, eight reflected waves, $v_{\mathrm{R}kmN}^{\mathrm{J1}}$ ($N = 2$ and $k = [1, 4]$), and eight transmitted waves, $v_{\mathrm{T}kmN}^{\mathrm{J1}}$, are generated on the interface of J1. Repeatedly, the new transmitted waves caused from J1 propagating in Zone I will spread downward from the joint as the same as $v_{\mathrm{Rp}0}^{\mathrm{J1}}$ and $v_{\mathrm{Rs}0}^{\mathrm{J1}}$. They are the components of the reflected waves from J1 and expressed as

$$v_{\mathrm{R}m}^{x_i}(x,t) = v_{\mathrm{T}kmN}^{\mathrm{J1}}(t) \quad (21)$$

where the abscissa x can be easily obtained according to the geometric relationship shown in Fig. 1. If the calculated x is greater than x_m, i.e., beyond the monitoring scope, the induced wave and the later propagation process will be ignored. The angles between the new transmitted waves and the vertical direction are expressed as

$$\theta_{\mathrm{R}m}^{x_i}(x) = \theta_{\mathrm{T}kmN}^{\mathrm{J1}} - \alpha_1. \quad (22)$$

Hence, the vertical and horizontal components of each transmitted wave can be expressed as

$$\begin{bmatrix} v_{\mathrm{Rp}y}^{x_i}(x,t) \\ v_{\mathrm{Rp}x}^{x_i}(x,t) \end{bmatrix} = v_{\mathrm{Rp}}^{x_i}(x,t) \cdot \begin{bmatrix} -\cos\theta_{\mathrm{Rp}}^{x_i}(x) \\ \sin\theta_{\mathrm{Rp}}^{x_i}(x) \end{bmatrix} \quad (23)$$

$$\begin{bmatrix} v_{\mathrm{Rs}y}^{x_i}(x,t) \\ v_{\mathrm{Rs}x}^{x_i}(x,t) \end{bmatrix} = v_{\mathrm{Rs}}^{x_i}(x,t) \cdot \begin{bmatrix} -\sin\theta_{\mathrm{Rs}}^{x_i}(x) \\ -\cos\theta_{\mathrm{Rs}}^{x_i}(x) \end{bmatrix}. \quad (24)$$

The new reflected waves from J1 continue to propagate toward J2. Repeatedly, multiple reflections take place between J1 and J2. Each wave impinging on J2 or J1 can be derived and expressed as Eqs. (14) and (19), respectively, where $N > 2$. As a result, more transmitted waves are generated and propagate in Zone III, indicated as $v_{\mathrm{T}m}^{x_i}(x,t)$. Similarly, more new reflected waves are generated in Zone I, which can be expressed as $v_{\mathrm{R}m}^{x_i}(x,t)$. Equations (17) and (18) show the vertical and horizontal components of each wave propagating upward away from J2, and Eqs. (23) and (24) show the components of each wave propagating downward from J1.

2.4 Wave Propagation Equation

Once an incident wave impinges on one of the two non-parallel joints, the transmitted and reflected waves generated from the joints propagate along various directions, which results in a complicated wave field. For any point in the area, a number of P- and S-waves with different propagating paths successively arrive at the location of the point, as shown in Fig. 3. Each wave is induced by one transmission or multiple reflections of the initial incident P-wave.

If the horizontal distance between two adjacent particles is defined to be Δx, there are limited particles within the monitoring scope, i.e., $x_i \in (x_0, x_m)$. The symbol q is adopted to denote the number of particles and $q = \mathrm{int}[(x_m - x_0)/\Delta x]$.

The initial condition is that any point x_i within the monitoring scope is not disturbed before the incident P-wave impinges on J1. At this moment, no transmitted or reflected waves are generated.

As the two joints are not parallel, the reflected waves generated from J1 or J2 always propagate along different directions. The incident P-wave impinging on different points on J1 may cause disparate transmitted waves at one point on J2. The transmitted waves also propagate along different directions. When the wave field is considered, the final transmitted wave is actually the sum of transmitted waves separately caused by the incident wave impinging on all points with abscissa ranging from x_1 to x_q. For a
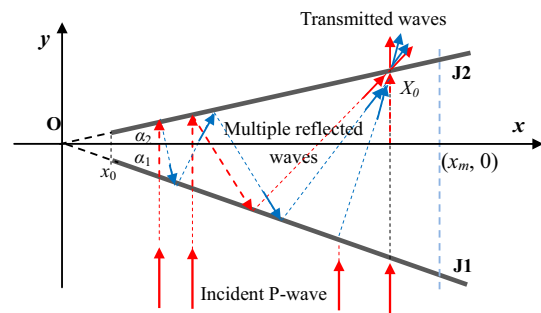

Fig. 3 Schematic view of P-wave propagation between two non-parallel joints

certain point on J2 with abscissa X_0, the vertical and horizontal components of the final transmitted wave can be expressed as

$$v_{Te}(X_0, t) = \sum_{j=1}^{q} v_{Tpe}^{x_j}(x, t)|_{x=X_0} + \sum_{j=1}^{q} v_{Tse}^{x_j}(x, t)|_{x=X_0} \qquad (25)$$

where $v_{Te}(X_0)$ ($e = y$ or x) are the vertical and horizontal components of the final transmitted wave at the point X_0. The vertical and horizontal components of the reflected wave from one point on J1 with abscissa X_0 can also be derived similarly, except that the subscript 'T' is replaced by 'R' in Eq. (25).

We define the vertical and horizontal components of the transmission coefficient, T_y and T_x, as the ratio of the amplitudes between the transmitted and incident waves, and vertical and horizontal components of the reflection coefficient, R_y and R_x, as the ratio of the amplitudes between the reflected and incident waves, i.e.,

$$T_e(X_0) = \frac{\max|v_{Te}|}{\max|v_0|}, \quad R_e(X_0) = \frac{\max|v_{Re}|}{\max|v_0|} \qquad (26)$$

3 Verification

In this section, the solutions obtained by the proposed theoretical method are compared with the numerical simulation results. This also serves as a verification of the proposed approach. In this study, the UDEC software is employed to simulate wave propagation across two non-parallel joints. The numerical model for a rock mass containing two non-parallel joints is shown in Fig. 4. The model is taken as 150×50 m, and it is symmetric on line

OO'. Both of the angles between the joints and the horizontal direction are 5°, i.e., $\alpha_1 = \alpha_2 = 5°$. Viscous boundaries are employed for the block boundaries along both directions of axes x and y. The linearly elastic model is adopted to describe the mechanical behavior of joints.

In the numerical model, the incident wave applied at the bottom of the model is a half-cycle sinusoidal P-wave with mathematical function of $v_0 = A_I \sin 2\pi f t$, where the amplitude A_I is 1 m/s, the frequency f is 50 Hz, and the duration t ranges from 0 to 0.01 s. The basic parameters for the rock and the joints are as follows: rock density ρ is 2650 kg/m^3, P-wave velocity c_p is 5830 m/s, and shear wave velocity c_s is 2940 m/s (Zhao 1996). The symbols K_n and K_s denote the normalized normal and tangential stiffness of the joints, respectively, and $K_n = k_n/(z_p\omega)$, $K_s = k_s/(z_s\omega)$, and $K_n = K_s$, where $\omega = 2\pi f$. The stiffness of two joints is assumed to be identical, i.e., $K_{n1} = K_{n2} = K_n$.

To distinguish the incident and transmitted waves, five monitoring points are chosen and shown in Fig. 4. The monitoring point A is located in the middle-lower part of the model to record the incident wave. The other four monitoring points, denoted as B, C, B′ and C′, are located on the upper interface of J2, where the points B and C and the points B′ and C′ are in the right and left parts of the model, respectively. The abscissas of the five points, A, B, C, B′ and C′, are $X_0 = 0$, 25, 50, −25 and −50 m, respectively. The ordinate of each monitoring point can be calculated from the geometrical condition shown in Fig. 1. From the velocity histories of the four points, the velocity components of transmitted waves along the x- and y-axis are recorded, as shown in Fig. 5. The analysis results for points B and C are also calculated based on the proposed theoretical method. Figure 5 illustrates the relationships
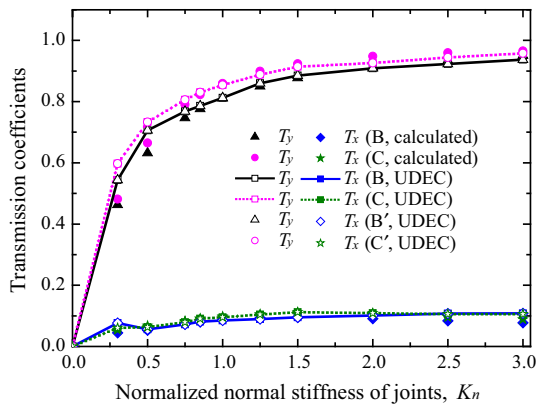

Fig. 4 Schematic view of the UDEC model
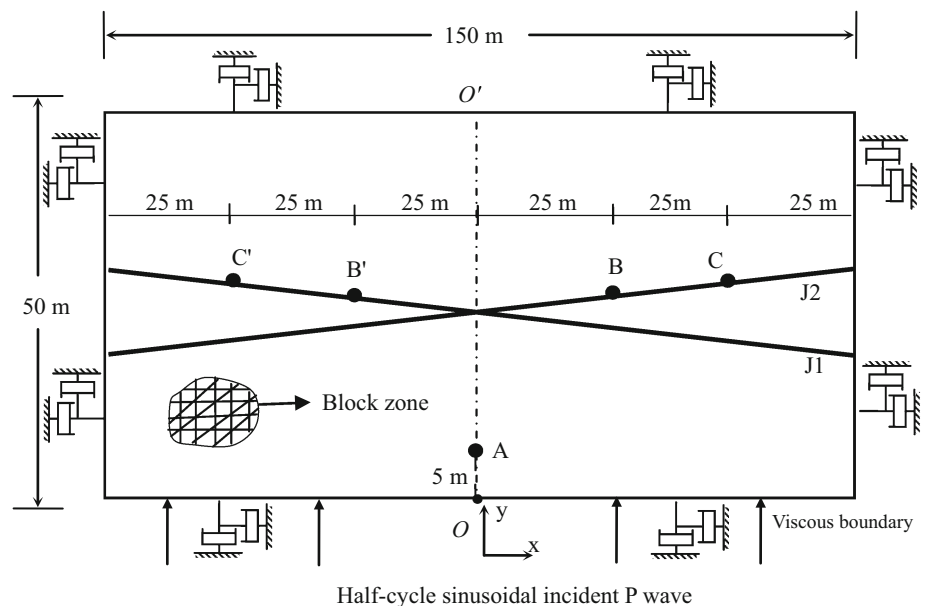
Fig. 5 Comparison between results based on present analytical approach and UDEC calculation

between the transmission coefficients, T_y and T_x, with the normalized normal stiffness of joints, K_n.

By comparison between the simulation and analytical results, it is found that the transmission coefficients obtained from UDEC modeling are very close to the results calculated from Eq. (26). The reason to cause the error between the theoretical and numerical methods is that the effect of the left part and interaction point of the joints on the transmission is not taken into account in the theoretical analysis. However, we show in Fig. 5 that the error is so tiny that it can be ignored. It indicates that the method proposed in this paper is effective and feasible to study wave propagation across two intersecting or non-parallel joints with the dihedral angle of 10°. Moreover, for a symmetric model situation, a half analytical model as illustrated in Fig. 3 can be adopted to analyze wave propagation accurately.

4 Discussion

Parametric studies will be conducted in this section to investigate the influences of the position of point on joints, the joint stiffness, the joint angle and the incident wave frequency on wave propagation across two non-parallel joints using the theoretical approach.

4.1 Limitations of the Approach

It should be noted that the proposed approach can only be applied to body wave propagation across non-parallel joints, that is, the emergence angle of stress wave is less than the critical angle, i.e., $0 \leq \alpha < \theta_{\mathrm{pcr}}$ and $0 \leq \beta < \theta_{\mathrm{scr}}$, where $\theta_{\mathrm{pcr}} = 90°$ and $\theta_{\mathrm{scr}} = \sin^{-1}(c_s/c_p)$. In this study, $\theta_{\mathrm{scr}} = 30.3°$. When the emergence angle of wave exceeds the range, the interface waves are generated and propagate along the interface of the joints. Hence, the incident angle

of P-wave is chosen to be less than 90°. In addition, when the angle between the joints is greater than 10°, in Zone II, the new incident angle of some S-waves caused by three-cycle reflection might be greater than the critical angle $\sin^{-1}(c_s/c_p) = 30.3°$, which causes the emergence angles of the new reflected and transmitted waves from the joint are not real-valued any more. Therefore, the current study only discusses the cases when the angle between two joints does not exceed to 10°.

4.2 Position of Point on Joints

Since the wave field is complicated, the transmitted waves generated from different positions of J2 propagate along different directions, so do the reflected waves from J1. Similar to the monitoring points on the upper interface of J2 shown in Fig. 4, some monitoring points are also placed on the lower interface of J1 to get the reflected wave from J1. The abscissa and ordinate of each monitoring point can be obtained from the geometrical relationship shown in Fig. 1.

The relationship between the transmission and reflection coefficients with the position of point on joints is shown in Fig. 6. In the calculation, both of the normalized normal and tangential stiffness of joints are assumed to be one. Besides, the angle between the two joints is taken as 5°. Three cases are considered, i.e., *Case 1* $\alpha_1 = 5°$ and $\alpha_2 = 0°$; *Case 2* $\alpha_1 = \alpha_2 = 2.5°$; and *Case 3* $\alpha_1 = 0°$ and $\alpha_2 = 5°$. The results corresponding to the three cases are shown in Fig. 6. It can be seen from the figure that the
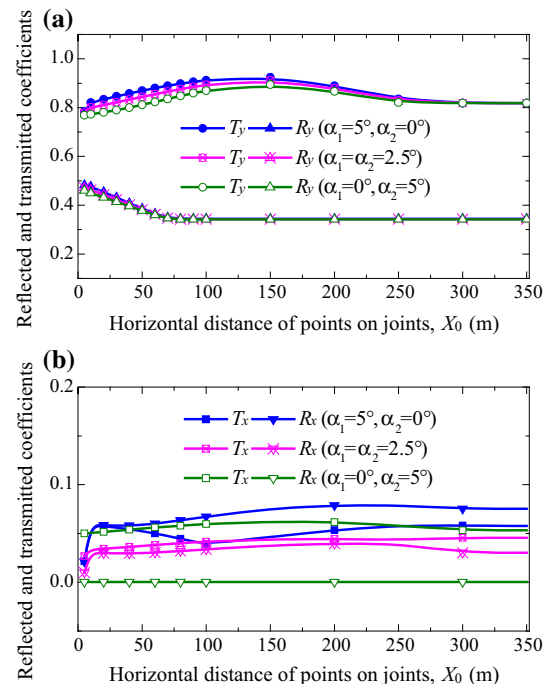

Fig. 6 Reflection and transmission coefficients at different monitoring points. **a** Vertical components. **b** Horizontal components

transmission and reflection coefficients vary with different positions of point. The variation trends of the transmission coefficient or reflection coefficient with the horizontal distance of the point in the three cases are very similar. Because of the small strike angle of the two joints, the values of T_x and R_x are relatively small compared with the components along y-direction and change slightly for the three cases. In addition, with the increase in the horizontal distance of the monitoring point, the transmission coefficient T_y increases firstly and then decreases, and finally tends to be stable, while the refection coefficient R_y decreases monotonously before turning to a constant value at around $X_0 = 80$ m. The maximum transmission coefficient T_y is recorded near $X_0 = 120$ m, and a convergence of T_y is observed near $X_0 = 300$ m. These two points divide the transmission coefficient into three regions: the increasing, decreasing and constant values. The increasing region is near to the intersecting point of two joints. In this region, the transmitted wave caused by the incident wave and multiple reflected waves between two joints makes the vertical component of amplitude of the transmitted wave increase and the horizontal component of the amplitude of the reflected wave decrease. The decreasing region is in the middle part, where the longer propagation distance and different spread directions of wave lead to a weak amplitude of transmitted wave, but a constant amplitude of reflected wave. In the constant-value region, the transmission and reflection coefficients are not influenced by the position of point on joints. Among the three cases, except the transmission coefficient T_x, the other coefficients for Case 1, i.e., $\alpha_1 = 5°$ and $\alpha_2 = 0°$, are almost greater than those for Cases 2 and 3, and the coefficients for Case 3 are the smallest. Comparison between Fig. 6a, b shows that the vertical components of either transmission or reflection coefficients are obviously greater than the horizontal components, which is caused by the present small value of joint strike angle.

4.3 Effect of Joint Stiffness

The incident wave and the basic parameters of joints and rocks shown in Sect. 3 will still be adopted in this and the following studies. The values of $z_s\omega$ and $z_p\omega$ are constant in this section. The normalized stiffness of joints, K_n, is taken into account to analyze the effect of joint stiffness on transmission and reflection coefficients.

For a point on J2 with $X_0 = 30$ m, the relation between the normalized normal stiffness of joint and the transmission and reflection coefficients is shown in Fig. 7, where the angles of two joints are equal to 5°, i.e., $\alpha_1 = \alpha_2 = 5°$. The normalized stiffness of J2 and J1 is kept the same, and there are $K_{n2} = K_{s2} = 1$ in Fig. 7a and $K_{n1} = K_{s1} = 1$ in Fig. 7b. It can be seen that each coefficient can be
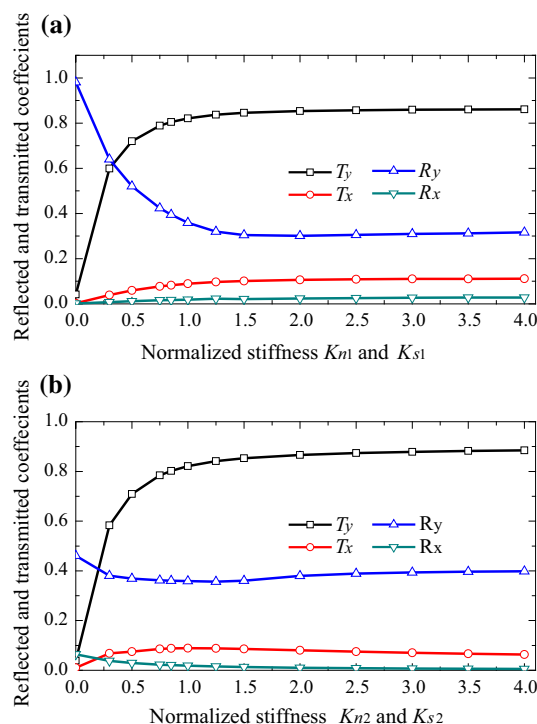

Fig. 7 Relation between reflection and transmission coefficients with normalized stiffness of joint. **a** Effect of stiffness of J1. **b** Effect of stiffness of J2

described as a function of the normalized joint stiffness. The influences of the normalized stiffness of J1 and J2 on the transmission and reflection coefficients are similar, but not identical. When the normalized stiffness of either J1 or J2 changes, the transmission coefficients, T_y and T_x, increase rapidly at small normalized stiffness, especially when K_n is <1, and then gently increase to be stable at a relative higher value of K_n. The variation of reflection coefficients with K_{n1} is different from those with K_{n2}, which is caused by the dissimilar wave fields around different positions of one joint. When K_{n1} approaches zero, there is no wave transmission from J1. Therefore, R_y tends to be 1 when the stiffness of J1 is zero, which means the incident wave is completely reflected from J1. If K_{n2} is equal to zero, only the waves arriving at J2 will be completely reflected, which results in R_y much less than that when K_{n1} is zero. In Fig. 7b, R_y shows a trend of slight decrease and then turns to be constant with increasing K_{n2}, while R_x gradually reduces to zero. This indicates that the portion of reflected waves caused by multiple reflections between two joints is reduced when J2 becomes stiff and waves transmission across J2 without any reflection.

4.4 Effect of Frequency of Incident Wave

The half-cycle sinusoidal P-wave is still used in this section as an incident wave, but with different frequencies. The
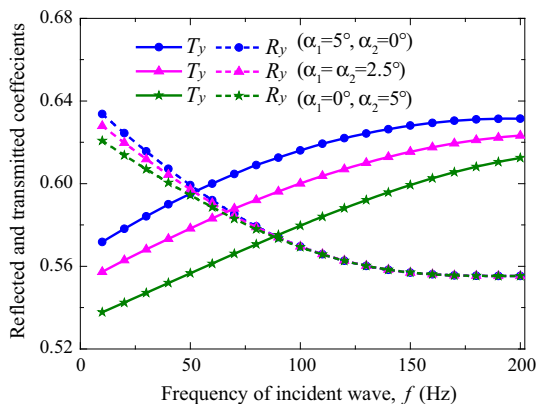
Fig. 8 Relation between reflection and transmission coefficients with frequency of incident wave

Fig. 9 Relation between reflection and transmission coefficients with joint strike

relationship between the reflection and transmission coefficients and the frequency of incident P-wave is illustrated in Fig. 8, where the monitoring points on the two joints are located at $X_0 = 30$ m. The angle between the two joints is 5°, i.e., $\alpha_1 + \alpha_2 = 5°$. Three cases are considered, i.e., *Case 1* $\alpha_1 = 5°$, $\alpha_2 = 0°$; *Case 2* $\alpha_1 = \alpha_2 = 2.5°$; and *Case 3* $\alpha_1 = 0°$, $\alpha_2 = 5°$. The tangential stiffness of the two joints is adopted as $k_{s1} = k_{s2} = 1.0$ GPa/m, and the normal stiffness is $k_{n1} = k_{n2} = k_{s1}c_p/c_s$. Since the horizontal components of the reflection and transmission coefficients, T_x and R_x, are smaller than the vertical components, T_y and R_y, only the effects of incident wave frequency on T_y and R_y are considered. It is shown in Fig. 8 that the transmission and reflection coefficients vary with increasing frequency. T_y in any of the three cases increases gradually, while the reflection coefficient, R_y, decreases first and then remains almost constant with increasing frequency of incident wave. The phenomenon indicates that the joint is like a filter to filter out stress waves with high frequency. The transmission coefficient, T_y, in Case 1 is the greatest, and T_y in Case 3 is the smallest if the frequency of incident wave is given. Different to the transmission coefficients, the reflection coefficients for the three cases are very close.

4.5 Effect of Joint Strike Angle

Figure 9 shows the relationship between the transmission and reflection coefficients with the joint strike angle, where J1 or J2 in parentheses means that the strike angle of the joint varies. When the influence of the angle of J1 is investigated, the angle of J2 is assumed as $\alpha_2 = 5°$; on the contrary, the angle of J1 remains at $\alpha_1 = 5°$ when the influence of the angle of J2 is studied. The monitoring points on the two joints are set at $X_0 = 30$ m. It is shown in Fig. 9 that the variation trend of each coefficient with the joint angle is not the same within the scope of $\alpha \in (0°, 10°)$. When the angle of J1 increases,
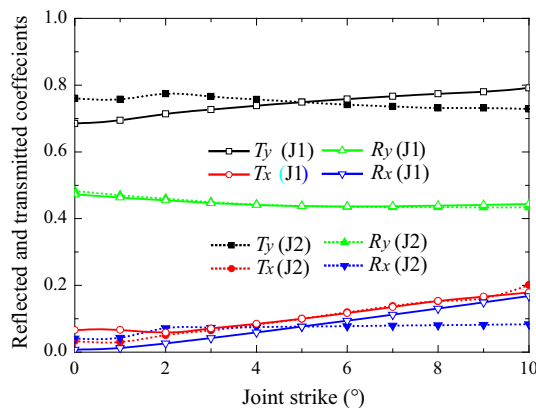
the transmission coefficients T_y and T_x gradually increase within a small variation range; the reflection coefficient R_y decreases, while R_x increases a little. In this study, as the strike angles of both joints are very small, the vertical components of the transmission and reflection coefficients are dominated by the transmitted and reflected P-waves, respectively. The horizontal components of the transmission and reflection coefficients are dominated by the transmitted and reflected S-waves. The value of T_y shown in Fig. 9 fluctuates with increasing strike angle of J2. This can be understood as less reflected waves arrive at the monitoring point and the time delay of each wave becomes longer, when the strike angle of J2 increases. The tendencies of T_x and R_y with the change of the strike of J2 are similar to those when the strike of J1 varies.

5 Conclusions

When an incident P-wave impinges on a rock mass with two non-parallel joints, wave propagation process is first analyzed. Then, the wave propagation equation is derived. The transmitted wave across J2 and the reflected wave from J1 are calculated thence. The proposed approach is proved to be effective in studying the characteristics of wave propagation through jointed rock mass when the influence of joint tip is not considered. The parametric studies show that both normal and tangential stiffness of each joint affect the transmission and reflection coefficients obviously. The frequency of incident wave has less influence on the reflection coefficient, which is different to the effect on the transmission coefficient. Besides, the transmission and reflection coefficients at different points are not the same. Since the two joints are non-parallel with each other, the wave field becomes quite complex. The reflected waves between the two joints have different

propagation directions, which change greatly with multiple reflection cycles. Hence, the transmitted waves become sensitive to the position of the second joint near to the intersecting point, so do the reflected wave from the first joint.

It should be noted that the present approach is only available for two non-parallel joints when the angle between two joints is small, that is, only body wave propagation is taken in account. The approach will be improved in our further study to analyze the effect of joint tips on wave propagation and to consider induced interface waves.

References

Achenbach JD (1973) Wave propagation in elastic solids. North-Holland, Amsterdam

Cai JG, Zhao J (2000) Effects of multiple parallel fractures on apparent attenuation of stress waves in rock masses. Int J Rock Mech Min Sci 37(4):661–682

Chen SG, Zhao J (1998) A study of UDEC modelling for blast wave propagation in jointed rock masses. Int J Rock Mech Min Sci 35(1):93–99

Cook NGW (1992) Natural joint in rock: mechanical, hydraulic and seismic behavior and properties under normal stress. Int J Rock Mech Min Sci Geomech Abstr 29(3):198–223

Crotty JM, Wardle LJ (1985) Boundary integral analysis of piecewise homogeneous media with structural discontinuities. Int J Rock Mech Min Sci 22(6):419–427

Cundall PA (1971) A computer model for simulating progressive large scale movements in blocky rock systems. In: Proceedings of the symposium on international society of rock mechanics, Nancy, France, vol. 1(ɪɪ-8), pp 129–136

Fan LF, Sun HY (2015) Seismic wave propagation through an in-situ stressed rock mass. J Appl Geophys 121:13–20

Goodman RE, Taylor L, Brekke TL (1968) A model for the mechanics of jointed rock. J Soil Mech Found Div 94:637–659

Li JC (2013) Wave propagation across non-linear rock joints based on time-domain recursive method. Geophys J Int 193(2):970–985

Li J, Ma G, Zhao J (2010) An equivalent viscoelastic model for rock mass with parallel joints. J Geophys Res 115(B3):1–10. doi:10.1029/2008JB006241

Li JC, Li HB, Ma GW, Zhao J (2012) A time-domain recursive method to analyze transient wave propagation across rock joints. Geophys J Int 188(2):631–644

Li JC, Zhao XB, Li HB, Chai SB, Zhao QH (2016) Analytical study for stress wave interaction with rock joints having unequally close–open behavior. Rock Mech Rock Eng 49(8):3155–3164

Ma GW, Fan LF, Li JC (2012) Nonlinear viscoelastic medium equivalence for stress wave propagation in a jointed rock mass. Int J Rock Mech Min Sci 50:11–18

Perino A, Orta R, Barla G (2012) Wave propagation in discontinuous media by the scattering matrix method. Rock Mech Rock Eng 45(5):901–918

Pyrak-Nolte LJ, Myer LR, Cook NGW (1990a) Transmission of seismic-waves across single natural fractures. J Geophys Res 95(B6):8617–8638

Pyrak-Nolte LJ, Myer LR, Cook NGW (1990b) Anisotropy in seismic velocities and amplitudes from multiple parallel fractures. J Geophys Res 95(B7):11345–11358

Schoenberg M (1980) Elastic wave behavior across linear slip interfaces. J Acoust Soc Am 68(5):1516–1521

Schoenberg M, Muir F (1989) A calculus for finely layered anisotropic media. Geophysics 54(5):581–589

Wu W, Li JC, Zhao J (2013) Seismic response of adjacent filled parallel rock fractures with dissimilar properties. J Appl Geophys 96:33–37

Wu W, Li JC, Zhao J (2014) Role of filling materials in a P-wave interaction with a rock fracture. Eng Geol 172:77–84

Zhao J (1996) Construction and utilization of rock caverns in Singapore, Part A: bedrock resource of the Bukit Timah granite. Tunn Undergr Space Technol 11(1):65–72

Zhao J, Cai JG (2001) Transmission of elastic P-waves across single fractures with a nonlinear normal deformational behavior. Rock Mech Rock Eng 34(1):3–22

Zhao XB, Zhao J, Cai JG (2006) P-wave attenuation across fractures with nonlinear deformational behaviour. Int J Numer Anal Methods Geomech 30(11):1097–1112

Zhao XB, Zhao J, Cai JG, Hefny AM (2008) UDEC modeling on wave propagation across fractured rock masses. Comput Geotech 35(1):97–104

Zhu JB, Zhao XB, Li JC, Zhao GF, Zhao J (2011) Normally incident wave propagation across a joint set with the virtual wave source method. J Appl Geophys 73:283–288

Zhu JB, Zhao XB, Wu W, Zhao J (2012) Wave propagation across rock joints filled with viscoelastic medium using modified recursive method. J Appl Geophys 86:82–87

Zhu JB, Deng XF, Zhao XB, Zhao J (2013) A numerical study on wave transmission across multiple intersecting joint sets in rock masses with UDEC. Rock Mech Rock Eng 46(6):1429–1442